

Screening of long-range Coulomb interactions in the quasi two-dimensional extended Hubbard model: A combined quantum Monte Carlo and Feynman diagram study

H.-B. Schüttler^{1,2}, C. Gröber³, H. G. Evertz^{3,4}, and W. Hanke^{2,3}

¹ *Center for Simulational Physics, Department of Physics and Astronomy, University of Georgia, Athens, Georgia 30602*

² *Institute for Theoretical Physics University of California, Santa Barbara, California 93106, USA*

³ *Institut für Theoretische Physik, Am Hubland, Universität Würzburg, D-97074 Würzburg, Germany*

⁴ *Institut für Theoretische Physik, Technische Universität Graz, 8010 Graz, Austria*

(April 17, 2001)

By combining fermion quantum Monte Carlo (QMC) simulations with diagrammatic theory, we have calculated the dielectric screening and the screened electron-electron interaction potential in a quasi two-dimensional extended single-band Hubbard model for cuprate superconductors, with and without a long-range ($1/r$) extended Coulomb interaction potential, at and near band-filling $\frac{1}{2}$. Our results for the insulating dielectric screening in the $\frac{1}{2}$ -filled band case indicate that the Hubbard conduction electron system contributes only a minor fraction, $\Delta\epsilon \cong 0.9$, of the total observed in-plane electronic dielectric constant of the cuprates, $\epsilon_{\infty\parallel} \cong 4.7$. With increasing hole doping concentration x , the extended ($1/r$ -) part of the Coulomb interaction potential is rapidly suppressed by the metallic screening, due to doping induced charge carriers. Surprisingly, near $x \sim 5\%$, the low-frequency component of the screened potential V_S changes sign and becomes attractive at 1st neighbor and more extended distances in the CuO_2 -plane. The 1st neighbor screened potential reaches maximum attraction strength at dopings $x \sim 13 - 15\%$ and becomes repulsive again at larger dopings, for $x \sim 23 - 25\%$. Similar results are found for the screened potential of the pure 2D Hubbard model, without extended Coulomb interaction terms, suggesting that the extended Coulomb terms do not qualitatively alter the local screening physics of the doped Hubbard electron system. When included exactly in the screening calculation, the 1st neighbor extended Coulomb term enhances the on-site and 1st neighbor overscreening attraction already present in the pure Hubbard model at finite doping. Our results are potentially relevant for the question of the d -wave pairing mechanism in the cuprates, since they suggest that the screened extended Coulomb interaction potential does not only not suppress a d -wave pairing state but, due to the overscreening, could actually increase the d -wave attraction, in the 5 - 25% doping regime. Our results may also have implications for the explanation of the isotope effect and its doping dependence in the cuprates. At larger dopings, $x > 15\%$, the screened potential becomes attractive even on-site, suggesting the possibility that the screened potential could support or enhance s -wave pairing in the high-doping regime. We also give a rigorous analytical proof that the screened on-site interaction must become attractive near half-filling in the repulsive large- U -limit of both the pure Hubbard and the extended Hubbard single-band model. We present a simple physical interpretation of this seemingly paradoxical result in terms of the retardation effects which are inherent in the screening of an instantaneous repulsive interaction potential. We also point out that on-site overscreening implies singularities in the imaginary-frequency dependence of the irreducible polarization insertion and its 3-point vertex function.

I. INTRODUCTION

In the cuprate high- T_c superconductors, the strong, on-site Hubbard- U Coulomb repulsion is believed to prevent conventional on-site Cooper pair formation. This long-standing theoretical dictum is now supported by experimental evidence, obtained in several cuprate materials, for a non- s -wave pairing state, of $d_{x^2-y^2}$ -symmetry.¹⁻³ A d -wave pairing state implies a spatially extended Cooper pair wavefunction, involving electrons paired at 1st neighbor or larger lattice distances. Such a non- s -wave state is impervious to the on-site U -repulsion, but it can still be suppressed by the extended part (1st, 2nd, ... neighbor) of the electron-electron Coulomb repulsion. The bare strength of this extended Coulomb potential

may be quite substantial in the cuprates. For any proposed microscopic model of the cuprates, it is therefore crucial to demonstrate that the model can support a d -wave pairing state near $\frac{1}{2}$ -bandfilling and that such a pairing state is robust against extended Coulomb repulsions.

In the present paper, we combine diagrammatic and quantum Monte Carlo (QMC) methods to study both the insulating dielectric screening at band-filling $\frac{1}{2}$ and, as a function of doping, the screened electron-electron interaction potential near the $\frac{1}{2}$ -filled band limit within the framework of a quasi two-dimensional (2D) Hubbard model with three-dimensional (3D) extended $1/r$ Coulomb interactions. In the $\frac{1}{2}$ -filled band case, our results suggest that the insulating Hubbard electron system

contributes only a minor fraction, $\Delta\epsilon \cong 0.9$, to the total observed electronic dielectric constant of the cuprates, $\epsilon_\infty \cong 4.7$, with most of the electronic dielectric screening being provided by non-Hubbard “background” electrons which are not explicitly included in the conventional single-band Hubbard description of the cuprates. In comparing to the observed values for the dielectric constant, we can thus obtain an estimate for the strength of the $1/|r|$ Coulomb interaction potential of the quasi 2D Hubbard electron system. At finite doping, we find that screening due to the doping induced “metallic” charge fluctuations causes the screened electron-electron interaction potential V_S to become attractive. At low doping concentrations x , this “overscreening” effect reverses the sign of the spatially extended part of V_S , giving rise to a 1st neighbor attraction in the 5 – 25% doping range, with a attraction strength maximum near $x = 15\%$. At larger x , even the on-site part of V_S turns attractive, for $x \gtrsim 15\%$. We give a rigorous analytical proof for the existence of this on-site overscreening effect and show that it is intrinsically a doping induced large- U effect of Hubbard systems near band-filling $\frac{1}{2}$. Possible implications of these overscreening effects for superconducting pairing instabilities in the 2D Hubbard and quasi-2D extended Hubbard model are also discussed.

The remainder of the paper is organized as follows: In Section II, we describe our model and outline the basic approach of combining QMC simulations with diagrammatic theory. In Section III, we present our calculation of the dielectric constant in the $\frac{1}{2}$ -filled Hubbard electron system and estimate the “bare” strength of the extended $1/|r|$ Coulomb interaction, by comparing to experimentally observed values in insulating cuprate parent compounds. In Section IV, we present our results for the on-site and 1st neighbor component of the screened Coulomb potential in the 2D Hubbard and quasi-2D extended Hubbard model. In Section V, we present an exact proof for the existence of on-site overscreening in the asymptotic $U \rightarrow \infty$ limit and discuss its implications for the analytical structure of the irreducible polarization insertion and its underlying vertex function. In Section VI, we speculate on possible implications of overscreening for the superconducting pairing instabilities of the 2D Hubbard and quasi-2D extended Hubbard model. Section VII contains a brief summary.

II. MODEL AND COMBINED DIAGRAMMATIC QUANTUM MONTE CARLO APPROACH

Both theoretical (bandstructure) calculations and experimental observations, specifically the highly anisotropic electronic transport properties of the cuprates, suggest that their electronic structure is close to two-dimensional and it is a reasonable first approximation to neglect interlayer electronic hybridization effects. However, the dielectric screening in the undoped insulating parent compounds

is far less anisotropic, with observed dielectric constants of quite similar magnitude parallel and perpendicular to the CuO_2 -layer directions. This suggests that the extended $1/r$ part of the electronic Coulomb repulsion is by no means confined to a single CuO_2 -layer and that the full 3D interaction potential may have to be taken into account. We therefore start from an extended Hubbard Hamiltonian of the form⁴

$$H = \sum_{j,\ell} \left(\frac{1}{2} V(r_{j\ell}) n_j n_\ell - \sum_{\sigma} t_{j\ell} c_{j\sigma}^\dagger c_{\ell\sigma} \right) \equiv H_V + H_t, \quad (1)$$

with $c_{j,\sigma}^\dagger$ creating an electron of spin $\sigma = \uparrow, \downarrow$ at Cu -site r_j in a three-dimensional (3D) crystal of stacked CuO_2 layers, $n_j = \sum_{\sigma} c_{j\sigma}^\dagger c_{j\sigma}$ and $r_{j\ell} = r_j - r_\ell$. H_t includes only an in-plane 1st neighbor hybridization t and the chemical potential μ . Some preliminary results including a 2nd neighbor hybridization t' have also been obtained. The 3D Coulomb potential

$$V(r) = U\delta_{r,0} + \frac{e^2}{\epsilon_B |r|_{\min}} (1 - \delta_{r,0}) \equiv U\delta_{r,0} + V_e(r) \quad (2)$$

includes the on-site repulsion U and an extended $1/|r|$ -part, V_e , with a dielectric constant ϵ_B to account for screening by the insulating background not explicitly included in H , that is “non-Hubbard” electrons in lower filled bands and, possibly, phonon degrees of freedom. On a finite $L^{(1)} \times L^{(2)} \times L^{(3)}$ lattice with periodic boundary conditions and primitive unit vectors $r^{(\alpha)}$, having linear dimension of $L^{(\alpha)}$ unit cells in the $r^{(\alpha)}$ -direction for $\alpha = 1, 2, 3$, we define

$$|r|_{\min} = \min_{m_1, m_2, m_3} \left| r - \sum_{\alpha=1}^3 m_\alpha L^{(\alpha)} r^{(\alpha)} \right| \quad (3)$$

with the m_α taken over all integers, to ensure proper periodicity of $V(r)$.

The exact screened potential V_S , the exact irreducible polarization insertion P and the exact density correlation function χ of the full Hamiltonian (1) are related by⁵

$$\begin{aligned} V_S(q, i\omega) &= [1 - V(q)P(q, i\omega)]^{-1} V(q) \\ &= V(q) - V(q)\chi(q, i\omega)V(q), \end{aligned} \quad (4)$$

where $V(q)$ denotes the lattice Fourier sum over $V(r)$ and

$$\begin{aligned} \chi(q, i\omega) &= \frac{1}{N} \sum_{j,\ell} \int_0^\beta d\tau e^{i\omega\tau - iq \cdot r_{j\ell}} \langle \Delta n_j(\tau) \Delta n_\ell(0) \rangle \\ &\equiv -P(q, i\omega) [1 - V(q)P(q, i\omega)]^{-1} \end{aligned} \quad (5)$$

at wavevectors q , Matsubara frequencies $i\omega$ and temperature $T \equiv 1/\beta$ for lattice size N with $\Delta n_j \equiv n_j - \langle n_j \rangle$.⁵

Here, $\langle \dots \rangle$ and $\dots(\tau)$ denote, respectively, thermal averaging and imaginary-time evolution with respect to H . Note that V_S and P depend on the choice of representation for H_V . Eqs. (4,5) are based on the diagrammatic expansion in the *charge* representation where the U -term is written as $\frac{U}{2} \sum_j n_j^2$, rather than the more familiar *spin* representation $U \sum_j n_{j\uparrow} n_{j\downarrow}$. While both are equivalent when all diagrams are summed exactly to all orders, the former, as we will discuss, may offer some advantages for approximate diagram resummations.

The basic idea of our QMC approach is to calculate V_S , via Eq. (4), from the polarization insertion P which, in turn, is extracted, via Eq. (5), from QMC results for the density correlation function χ . In order to include the full 3D extended Coulomb repulsion into this approach, we treat only a certain short-range portion of $V(r)$, denoted by $V_o(r)$, exactly, by QMC methods. The remaining weaker, but long-range part of V , denoted by $V_f(r) \equiv V(r) - V_o(r)$, is then handled perturbatively.

By retaining only in-plane terms in V_o , the QMC simulation can be restricted to a single 2D layer. We thus calculate, by QMC, the density correlation function

$$\begin{aligned} \chi_o(q, i\omega) &= \frac{1}{N} \sum_{j,\ell} \int_0^\beta d\tau e^{i\omega\tau - iq \cdot r_{j\ell}} \langle \Delta n_j(\tau)_o \Delta n_\ell(0)_o \rangle_o \\ &\equiv -P_o(q, i\omega) [1 - V_o(q) P_o(q, i\omega)]^{-1} \end{aligned} \quad (6)$$

for the QMC Hamiltonian

$$H_o \equiv H_{V_o} + H_t \quad (7)$$

on a single 2D CuO_2 -plane, with the interaction potential V in Eq. (1) replaced by V_o . Here, $\langle \dots \rangle_o$ and $\dots(\tau)_o$ denote, respectively, thermal averaging and imaginary-time evolution with respect to H_o and P_o is the exact irreducible polarization insertion of H_o ⁵ which can be extracted from the QMC results for χ_o via Eq. (6).

Our essential approximation is to replace the exact P of the full Hamiltonian H in Eqs. (4,5) by P_o , *i.e.*, we set

$$P(q, i\omega) \cong P_o(q, i\omega) = [V_o(q) - 1/\chi_o(q, i\omega)]^{-1} \quad (8)$$

in Eqs. (4) and (5). All renormalizations of P due to the short-range part of the interaction potential, V_o , are thus included exactly, to all orders of V_o . Renormalizations due to the weaker long-range part V_f are neglected in P , but approximately included in V_S , via Eq. (4), and in χ , via Eq. (5), *i. e.* by setting $V_S(q, i\omega) \cong [1 - V(q) P_o(q, i\omega)]^{-1} V(q)$ and $\chi(q, i\omega) \cong -P_o(q, i\omega) [1 - V(q) P_o(q, i\omega)]^{-1}$. Note that this approximation for P becomes exact if we replace H by H_o , as, *e.g.*, in our calculations of P and V_S for the pure 2D Hubbard model discussed below.

As a simple cuprate system, we consider $La_{2-x}Sr_xCuO_4$, with a body-centered tetragonal (*bct*) 3D model crystal structure, in-plane lattice constant $a = 3.80\text{\AA}$, inter-layer spacing $d = 6.62\text{\AA}$ ⁶, $t = 0.35eV$ and $U = 8t^4$. (Small orthorhombic or larger-unit-cell

tetragonal distortions from this idealized structure are neglected.) Note that the foregoing values for U and t are consistent with the values derived by the systematic mapping of the low-energy Hilbertspace of the three-band onto the single-band Hubbard model.⁴ The values of U and t are also consistent with (and, essentially, determined by) the observed values of the antiferromagnetic exchange constant $J \cong 0.13eV$ and of the Mott-Hubbard charge excitation gap $\Delta_{MH} \cong 1.8 - 2.6eV$ in the undoped La_2CuO_4 parent compound.⁴

Using standard finite-temperature fermion determinant QMC methods, χ_o is simulated with up to 2×10^7 MC sweeps and typically $\lesssim 0.5\%$ statistical error on 6×6 , 8×8 and 10×10 2D square lattices with periodic boundary conditions at $\beta \equiv 1/T$ up to $\beta t = 10$, with imaginary-time step $\Delta\tau \equiv \beta/L_\tau \leq 0.0625t^{-1}$ where L_τ is the Trotter number. In most simulations, we use for H_o the pure Hubbard model with

$$V_o(r) = U\delta_{r,0} \quad (9)$$

In order to explore the effects arising from inclusion of extended V -terms in the polarization insertion P_o , we have also performed a few simulations for the 1st neighbor extended Hubbard model, with

$$V_o(r) = U\delta_{r,0} + V_1 \sum_{s \in \mathcal{N}_1} \delta_{r,s} \quad (10)$$

where

$$V_1 \equiv \frac{e^2}{\epsilon_B a} \quad (11)$$

is the strength of the bare in-plane 1st neighbor Coulomb repulsion and \mathcal{N}_1 denotes the set of in-plane 1st neighbor lattice vectors, $s = (\pm a, 0, 0)$ and $(0, \pm a, 0)$.

III. DIELECTRIC SCREENING IN THE $\frac{1}{2}$ -FILLED MOTT-HUBBARD INSULATOR

Our first objective is to calculate the dielectric constant of the insulator from our model and thereby obtain an estimate for the background screening ϵ_B [in Eq. (2)] from the measured long-wavelength external field dielectric tensor $\tilde{\epsilon}_{\text{ex}}(\omega)|_{q \rightarrow 0}$ in the undoped, insulating La_2CuO_4 material.^{7,8} Note here that the observed $\tilde{\epsilon}_{\text{ex}}(\omega)|_{q \rightarrow 0}$ contains contributions from both the conduction electron system, explicitly included in our Hubbard model description, *and* from the “background” electron and phonon degrees of freedom which are not explicitly included in our single-band Hubbard description. Note also that in our simplified model, ϵ_B is represented as a momentum- and frequency-independent constant, *i.e.*, in effect the background is treated as a structureless homogeneous dielectric medium, down to atomic length scales. We should caution from the outset that such an

approach can provide only reasonable order of magnitude estimates.

In a more quantitative modeling approach, based *e.g.*, on a shell model representation of the insulating non-Hubbard electron and phonon background,⁹ one may include more realistically the momentum and frequency structure of ϵ_B . However, as discussed briefly below, the “local field” effects in such a model, arising from the momentum dependence of ϵ_B , will not qualitatively alter our main conclusions. Also, the frequency dependence of the electronic contribution to ϵ_B is likely of lesser importance, due to the high charge excitation energy scale of the background electrons which is expected⁴ to be in the several eV range, exceeding the Hubbard electron bandwidth $8t$. Via the phonon contribution to ϵ_B , on the other hand, the low phonon frequency scale $\Omega_{\text{ph}} \lesssim 0.1\text{eV} \ll 8t$, enters into the screening of the Coulomb interaction, and, along with it, isotopic mass dependence. This may have implications for the explanation of the isotope effect observed in the superconducting properties of the cuprates, especially in the underdoped regime, as discussed further in Section IV. However, as we will also explain in Section IV, neither the presence of the phonon contribution in ϵ_B nor its low frequency scale, will substantially alter the Hubbard electrons’ “metallic” screening at finite doping which is the central focus of the present paper.

Within the framework of our simplified background dielectric model, we obtain the longitudinal (scalar) dielectric function ϵ_{ex} from¹⁰

$$\frac{1}{\epsilon_{\text{ex}}(q, i\omega)} = \frac{1}{\epsilon_B} \left[1 - \frac{4\pi e^2}{\epsilon_B \mathcal{V}_c |q|^2} \chi(q, i\omega) \right] \quad (12)$$

at $i\omega = 0$. Here, \mathcal{V}_c denotes the 3D unit cell volume and as discussed above, $\chi = -P[1 - V(q)P]^{-1}$ from (5) with $P \cong P_o$. The components of the static dielectric tensor $\tilde{\epsilon}_{\text{ex}}$ in the long-wavelength limit can then be extracted from

$$\hat{e} \cdot \tilde{\epsilon}_{\text{ex}} \cdot \hat{e} = \lim_{|q| \rightarrow 0} \lim_{L \rightarrow \infty} \epsilon_{\text{ex}}(|q|\hat{e}, i\omega = 0) \quad (13)$$

for arbitrary unit vectors \hat{e} with L denoting the linear lattice size. Note here that it is crucial to take the thermodynamic limit $L \rightarrow \infty$ at finite $|q| > 0$ *before* taking the long-wavelength limit $|q| \rightarrow 0$.

Since the finite-system QMC simulations provide us with density correlation data $\chi_o(q, i\omega)$ only on a finite, discrete q -grid, some special care must be taken to extract the foregoing limits from the QMC data. To do so, we have developed a simple, physically motivated r -space embedding procedure which provides us with a continuous q -space interpolation and gives a reasonable approximation of $\chi_o(q, i\omega)$ in the thermodynamic limit. Our embedding procedure is based on the observation that, in the $\frac{1}{2}$ -filled limit at large U , $U \sim 8t$, and low temperature T , the single-layer density correlation function $\chi_o(r, i\omega)$ in r -space is actually of quite short range and, already on rather small lattices, exhibits very little finite-size dependence. Physically, this is simply a manifestation of

the fact that the charge excitation spectrum exhibits a large Mott-Hubbard gap, $\Delta_{\text{MH}} \sim U \gg t, T$. The Mott-Hubbard gap not only suppresses all charge correlations; it also endows them with a very short charge correlation length, ξ . In fact, from our QMC data taken on 8×8 lattices at $T = 0.1t$ we estimate ξ to be substantially less than the in-plane lattice constant a .

Based on this observation, we approximate $\chi_o^{(L)}(r, i\omega)$ for a large $L \times L$ square lattice by the QMC result $\chi_o^{(\text{QMC})}(r, i\omega)$, obtained on a smaller lattice of size $L_o \times L_o$, for those r -vectors which fall within the (properly symmetrized) boundaries of the smaller lattice; for r -vectors outside of those small-lattice boundaries, we simply set $\chi_o^{(L)}(r, i\omega)$ to zero. Specifically, for 2D lattice vectors $r \equiv (m_1 a, m_2 a)$ on the $L \times L$ “host” lattice, with integer m_1, m_2 and $|m_1|, |m_2| \leq L/2$, we set

$$\chi_o^{(L)}(r, i\omega) = w(r, L_o) \chi_o^{(\text{QMC})}(r, i\omega) \quad (14)$$

where, for even L_o ,

$$w(r, L_o) = \begin{cases} 1 & \text{if } |m_1| < L_o/2 \text{ and } |m_2| < L_o/2 \\ \frac{1}{2} & \text{if } |m_1| = L_o/2 \text{ and } |m_2| < L_o/2 \\ \frac{1}{2} & \text{if } |m_1| < L_o/2 \text{ and } |m_2| = L_o/2 \\ \frac{1}{4} & \text{if } |m_1| = L_o/2 \text{ and } |m_2| = L_o/2 \\ 0 & \text{otherwise} \end{cases} \quad (15)$$

In principle, we could also set the embedding weight factors $w(r, L_o)$ to zero for those lattice vectors which fall “on the boundary” (*i.e.* for $|m_1| = L_o/2$ or $|m_2| = L_o/2$), without noticeably changing our final results, since even for our small QMC lattices, our $\chi_o^{(\text{QMC})}(r, i\omega)$ are already negligibly small on the boundary. With the above choice of w , Eq. (15), we are ensuring that the large-lattice $\chi_o^{(L)}$ provides a “natural” interpolation of the small-lattice $\chi_o^{(\text{QMC})}$ in q -space, in the sense that, after Fourier transform, identically

$$\chi_o^{(L)}(q, i\omega) = \chi_o^{(\text{QMC})}(q, i\omega) \quad (16)$$

for those discrete 2D q -points $q \equiv (2\pi/a)(p_1/L_o, p_2/L_o)$, with integer p_1, p_2 , which lie on the discrete q -grid of the smaller $L_o \times L_o$ lattice.

An additional complication in extracting $\tilde{\epsilon}_{\text{ex}}$ from the QMC data arises from the fact that the QMC simulations are performed at finite temperature where the system exhibits a small, but non-zero, concentration of electron and hole charge carriers due to thermal excitation across the Mott-Hubbard gap. In our QMC simulations in the grand-canonical ensemble, these thermally excited carriers manifest themselves by the fact that

$$\chi_o^{(T)} \equiv \chi_o^{(L)}(q = 0, i\omega = 0) > 0 \quad (17)$$

i.e. at finite T there is a finite thermal fluctuation in the system’s total particle number. From QMC simulations at different temperatures, we have verified that this thermal carrier contribution to χ_o does indeed exhibit

the expected activated behavior, *i.e.*, roughly $\chi_o^{(T)} \sim \exp(-\Delta_{MH}/T)$. If included in the calculation of $\chi(q, i\omega)$ this finite $q = 0$ charge fluctuation would give rise to a “quasi metallic” singular contribution to the scalar dielectric function which would completely dominate the $q \rightarrow 0$ limit, with

$$\epsilon_{\text{ex}}(q, i\omega = 0) \sim \frac{4\pi e^2}{\mathcal{V}_c q^2} \chi_o^{(T)}. \quad (18)$$

Physically this reflects the fact that the thermally excited charge carriers are screening out any macroscopic Coulomb field with a finite screening length, which is simply a manifestation of the general principle that no physical system can be a true insulator at finite temperature.

To estimate the ($T = 0$) insulator contribution to χ_o , we thus subtract out the thermally activated carrier contribution and use as our χ_o -input into Eq. (8)

$$\chi_{o,\text{ins}}^{(L)}(q, i\omega) = \chi_o^{(L)}(q, i\omega) - \chi_o^{(T)} \delta_{i\omega,0} \quad (19)$$

to calculate $P_o(q, i\omega)$. With this subtraction, the resulting χ from Eq. (5) indeed, by construction, acquires the correct “insulating” long-wavelength behavior to give a finite ϵ_{ex} for $|q| \rightarrow 0$.

Taking the limit $L \rightarrow \infty$ on $\chi_{o,\text{ins}}^{(L)}$ and then expanding the resulting $\chi_{o,\text{ins}}^{(\infty)}$ around $q = 0$, we can write

$$\chi_{o,\text{ins}}^{(\infty)}(q, i\omega = 0) = \hat{e} \cdot \tilde{B} \cdot \hat{e} |q|^2 + \mathcal{O}(|q|^4) \quad (20)$$

for $q \equiv |q|\hat{e}$ with unit vector \hat{e} and with the cartesian components of the \tilde{B} -tensor given by

$$B_{\alpha\beta} = \frac{1}{2} \lim_{|q| \rightarrow 0} \frac{\partial^2 \chi_{o,\text{ins}}^{(\infty)}(q, i\omega = 0)}{\partial q_\alpha \partial q_\beta} \quad \text{for } \alpha, \beta = 1, 2, 3. \quad (21)$$

Inserting $\chi_{o,\text{ins}}^{(\infty)}(q, i\omega = 0)$ from Eq. (20) into Eq. (8), combining with Eqs. (5,12), taking the limit $|q| \rightarrow 0$ in Eq. (12) and comparing to Eq. (13), we get

$$\tilde{\epsilon}_{\text{ex}} = \epsilon_B \tilde{\mathbb{1}} + \frac{4\pi e^2}{\mathcal{V}_c} \tilde{B}. \quad (22)$$

With the cartesian coordinate axes chosen along the conventional tetragonal symmetry directions, only the diagonal components of \tilde{B} and $\tilde{\epsilon}_{\text{ex}}$ are non-zero with the in-plane component given by

$$\epsilon_{\parallel} \equiv \epsilon_{\text{ex},11} = \epsilon_{\text{ex},22} = \epsilon_B + \frac{4\pi e^2}{\mathcal{V}_c} B_{\parallel}. \quad (23)$$

Since, in our approximation, we do not include any interlayer charge correlations in χ_o , the out-of-plane (“ c -axis”) component of \tilde{B} vanishes and we get

$$\epsilon_{\perp} \equiv \epsilon_{\text{ex},33} = \epsilon_B, \quad (24)$$

i.e. the Hubbard electron system does not contribute to the c -axis dielectric screening.

From our QMC results for $\chi_o^{(QMC)}$ on a $L_o \times L_o = 8 \times 8$ lattice, embedded in large $L \times L$ lattices with L up to 512, we estimate B_{\parallel} , using Eq. (21), and from it the Hubbard electron system’s contribution to the in-plane dielectric constant

$$\Delta\epsilon \equiv \epsilon_{\parallel} - \epsilon_{\perp} = \frac{4\pi e^2}{\mathcal{V}_c} B_{\parallel}. \quad (25)$$

Using the pure on-site Hubbard potential, Eq. (9), as our interaction potential V_o in the QMC Hamiltonian, with the standard Hubbard model parameters stated in the previous section, we find $\Delta\epsilon \cong 0.70$ from QMC data obtained $T = 0.333t$ and $\Delta\epsilon \cong 0.93$ from QMC data obtained $T = 0.1t$. Note that this value of $\Delta\epsilon$ is independent of ϵ_B , since χ_o and B_{\parallel} depend only on the QMC Hamiltonian H_o which is independent of ϵ_B for the pure Hubbard case.

The slight ($\sim 25\%$) T -dependence of the foregoing $\Delta\epsilon$ result suggests that the thermal fluctuations, due to thermally excited carriers, are still noticeably (but not substantially) affecting the “insulating” charge correlations in the Mott-Hubbard insulator itself, at $T = 0.333t$. This is not entirely surprising since, *e.g.*, the thermal carrier subtraction $\chi_o^{(T)}$ at that T is about 10 – 20% of typical χ_o -values at typical non-zero $|q| \sim \pi/a$, *e.g.* $\chi_o^{(T)}/\langle \chi_o(q, i\omega = 0) \rangle_{BZ} \cong 0.15$ where $\langle \dots \rangle_{BZ}$ denotes the Brillouin zone average over q . However, it is reasonable to assume that the $T = 0.1t$ result approximates the $T = 0$ limit to within a percent or better, since the thermal carrier subtraction $\chi_o^{(T)}$ at $T = 0.1t$ is already 5 orders of magnitude smaller than, say, typical χ_o , *e.g.*, $\chi_o^{(T)}/\langle \chi_o(q, i\omega = 0) \rangle_{BZ} \cong 2 \times 10^{-5}$.

To explore the effects of including renormalizations due to extended Coulomb interactions in the polarization insertion P_o , we have also performed simulations for a $\frac{1}{2}$ -filled 1st neighbor extended Hubbard model, Eq. (10), with $V_1 = t = 0.35\text{eV}$ at $T = 0.333t$. The resulting change in $\Delta\epsilon$, $\delta\Delta\epsilon \equiv \Delta\epsilon|_{V_1=t} - \Delta\epsilon|_{V_1=0} \cong -0.014$, is only about 2% of $\Delta\epsilon$. Unfortunately, minus problems in the QMC simulations prevent us from extending these V_1 -dependent studies to lower T and/or more realistic larger V_1 -values, with, say, $V_1 = 2 - 3 \times t$. However, the foregoing result clearly suggests that the extended Coulomb effects on the polarization insertion are entirely negligible, at least as far as the long-wavelength limit at $\frac{1}{2}$ -filling is concerned.

The measured values for the dielectric tensor $\tilde{\epsilon}_{\text{ex}}(\omega)$ of undoped La_2CuO_4 in the static limit $\omega \rightarrow 0$ are $\epsilon_{0,\parallel} \equiv \epsilon_{\parallel}(\omega = 0) \cong 30 \pm 3$ for the in-plane component, and $\epsilon_{0,\perp} \equiv \epsilon_{\perp}(\omega = 0) \cong 25 \pm 3$ for the c -axis component.⁷ However, these values include a large, in fact, dominant phonon contribution.¹¹

The purely electronic contribution to the dielectric screening is observed at frequencies $\omega_\infty \sim 0.5 - 1\text{eV}$, which are well above the phonon spectrum $\Omega_{\text{ph}} \lesssim 0.1\text{eV}$, but at the same time still well below the electronic Mott-Hubbard charge gap $\Delta_{MH} \sim 1.5 - 2\text{eV}$. In this frequency regime, one finds approximately frequency independent values of $\epsilon_{\infty,\parallel} \equiv \epsilon_{\parallel}(\omega_\infty) \cong 4.73$ for the in-plane component, and $\epsilon_{\infty,\perp} \equiv \epsilon_{\perp}(\omega_\infty) \cong 4.56$ for the c -axis component.⁸ The corresponding anisotropy $\Delta\epsilon_\infty = \epsilon_{\infty,\parallel} - \epsilon_{\infty,\perp} \cong 0.2$ is substantially smaller than our estimated value $\Delta\epsilon = 0.9$. However, in our model estimate, we are assuming an isotropic background ϵ_B , whereas, in the real material, the background itself could also be anisotropic. If we generalize our model to allow for such a background anisotropy, we can estimate the background in-plane and c -axis components, $\epsilon_{B\parallel}$ and $\epsilon_{B\perp}$, for our model from the experimental ω_∞ -data and our calculated $\Delta\epsilon$. Namely, from the generalized Eqs. (23,24,25), $\epsilon_{B\parallel} = \epsilon_{\infty,\parallel} - \Delta\epsilon \cong 3.81$ and $\epsilon_{B\perp} = \epsilon_{\perp} \cong 4.57$, corresponding to a background anisotropy $\Delta\epsilon_B \equiv \epsilon_{B\parallel} - \epsilon_{B\perp} \cong -0.8$.

One of the main conclusions from the foregoing analysis is that the background degrees of freedom dominate the dielectric constant at $\frac{1}{2}$ -filling, with the Hubbard "conduction band" electrons contributing only about 25% to the total electronic dielectric constant, as observed in the ω_∞ frequency range. The other main conclusion is that both in the background dielectric screening and in the full dielectric screening (including Hubbard electrons), the anisotropy is insignificant, compared to the actual values of the dielectric tensor components. This conclusion holds equally well for the purely electronic contribution to the dielectric screening and for the phonon contribution, as evidenced by the nearly identical values of $\epsilon_{0\parallel} \sim 30$ and $\epsilon_{0\perp} \sim 25$ in the static limit. We will therefore in the following continue to work with an isotropic background model, with the electronic (ω_∞) value $\epsilon_B = \sqrt{\epsilon_{B\parallel}\epsilon_{B\perp}} \cong 4$ and the analogously obtained static ($\omega \rightarrow 0$) value $\epsilon_B \cong 27$, providing, respectively, reasonable lower and upper limits for ϵ_B .

From the estimated $\epsilon_B \cong 4$ (without phonons) or even $\epsilon_B \cong 27$ (including phonons), one obtains substantial 1st neighbor repulsion strengths of $V_1 \equiv e^2/(\epsilon_B a) \cong 0.95\text{eV} \cong 2.7t$ in the former and $V_1 \cong 0.14\text{eV} \cong 0.4t$ in the latter case. Thus, the extended part of the Coulomb potential, $V_e(r)$, appears to be indeed strong enough, that it could severely suppress extended (1st neighbor) pairing potentials which are commonly invoked in both phenomenological¹²⁻¹⁴ and microscopic¹⁵⁻¹⁸ scenarios of d -wave pairing.¹⁹ It is therefore of considerable interest to find out how this bare Coulomb interaction potential between the Hubbard electrons is modified due to the metallic screening generated by the doped Hubbard electron system itself. In the next section, we will turn to this question.

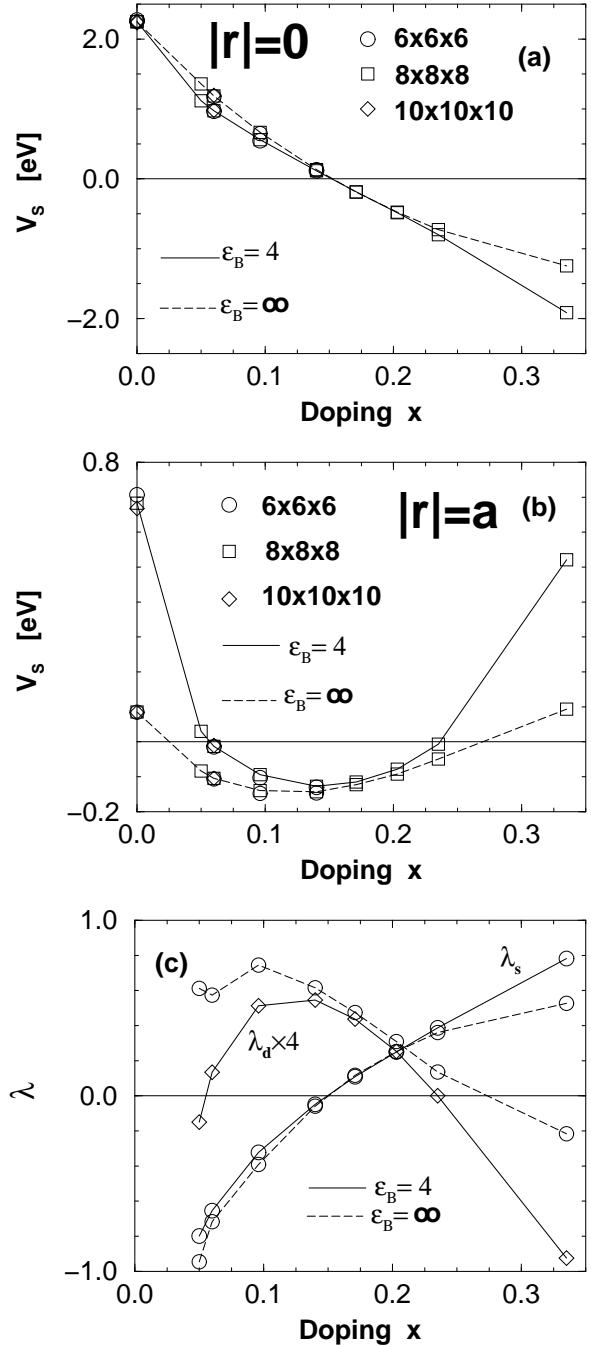


FIG. 1. Screened Coulomb potential $V_S(r) \equiv V_S(r, i\omega = 0)$ at (a) on site ($r = 0$) and (b) at in-plane 1st neighbor lattice vectors r and (c) Eliashberg λ -parameters for in-plane 1st neighbor $d_{x^2-y^2}$ and on-site/1st neighbor s -wave pairing, all plotted vs. hole doping concentration $x = 1 - \langle n_j \rangle$ at $\beta t \equiv t/T = 3.0$ and $\Delta\tau t = 0.0375$ for $\epsilon_B = 4$ (full lines) and $\epsilon_B = \infty$ (dashed lines). In (a) and (b), results are for La_2CuO_4 with bct lattices of sizes $6 \times 6 \times 6$, $8 \times 8 \times 8$ and $10 \times 10 \times 10$, with estimated QMC statistical uncertainties in V_S of less than 0.01eV. In (c), results are based on $8 \times 8 \times 8$ bct lattice data for V_S , extracted from 8×8 QMC data for χ_o . λ_d has been multiplied $\times 4$ for display.

IV. QMC RESULTS FOR V_S

In Fig. 1(a) and (b), we show results for $V_S(r, i\omega)$ at $i\omega = 0$, plotted *vs.* doping $x \equiv 1 - \langle n_j \rangle$ for the on-site ($r = 0$) and in-plane 1st neighbor r -vector in the quasi-2D extended Hubbard model on the La_2CuO_4 *bct* crystal structure with $\epsilon_B = 4$ and $\epsilon_B = \infty$. Note that the latter ϵ_B represents just the pure 2D Hubbard model, with the extended part of the Coulomb potential, V_e , set to zero. The results for V_S were extracted from QMC data for the single-plane density correlation function χ_o of the pure 2D Hubbard model, *i.e.*, with V_o given by Eq. (9), as explained in Section II, and with $V_S(r, i\omega)$ obtained from $V_S(q, i\omega)$ by Fourier transform over the finite-lattice 1st Brillouin zone. Since we are only interested in the short-distance behavior of V_S here, we have not attempted to embed our 2D χ_o -data in larger 2D lattices, as was done in the previous Section for the insulating dielectric function calculations. Rather, all results shown are for $L_o \times L_o \times L_o$ 3D lattices, using QMC data for χ_o obtained on corresponding $L_o \times L_o$ 2D lattices, with $L_o = 6, 8$, and 10.

As shown in Fig. 1(b) a small amount of doping suppresses the extended $1/|r|$ -repulsion for $r \neq 0$ and causes a sign change in the 1st neighbor and (not shown) in the 2nd and 3rd neighbor screened potential. Thus, $V_S(r)$ at short-range in-plane distances $r \neq 0$ becomes attractive, for x of order 5%, the attraction strength reaches a maximum at $x \sim 10 - 14\%$, and $V_S(r)$ turns repulsive again at $x \sim 23 - 28\%$.

As shown in Fig. 1(a), the on-site ($r = 0$) potential, while largely unaffected by screening at $x = 0$, is also rapidly suppressed with increasing x and it also becomes attractive at larger doping, near $x \cong 15\%$. Over the doping range studied, the screened on-site potential varies monotonically with x , in contrast to the extended ($r \neq 0$) part of V_S .

As a function of ϵ_B , V_S varies generally monotonically, in the directions indicated in Figs. 1(a) and (b). If we increase ϵ_B from 4 to the upper estimated value of $\epsilon_B = 27$, we find that the resulting V_S will be within 1 – 2% of the $\epsilon_B = \infty$ (pure 2D Hubbard) results shown in Figs. 1(a) and (b). Overall, in comparing the quasi-2D extended Hubbard model with $\epsilon_B = 4$ to the pure 2D Hubbard model ($\epsilon_B = \infty$), we note that all the foregoing results are qualitatively unaffected by the extended Coulomb repulsion. The primary effect of the extended Coulomb terms is to move the 1st neighbor V_S slightly in the repulsive direction, thereby suppressing the maximal 1st neighbor attraction strength in Fig. 1(b) by less than 10%. In addition, the extended Coulomb interaction shifts the “optimal” doping, where the 1st neighbor attraction maximum occurs, from $x \cong 10\%$ in the pure 2D Hubbard model to $x \cong 13\%$ in the quasi-2D extended Hubbard model with $\epsilon_B = 4$. The screened on-site potential is shifted slightly in the attractive direction, but, again, for doping concentrations up to 20%, the effect is

typically smaller than 10%.

These results suggest that, despite the substantial strength of the bare extended Coulomb potential V_e at near-neighbor distances, the local screened potential in the Hubbard electron system at finite doping is largely unaffected by extended Coulomb interactions. Recall from the previous section that the Hubbard electrons are largely ineffective in providing dielectric screening in the $\frac{1}{2}$ -filled insulator. By contrast, the results in Fig. 1 suggest that the Hubbard electrons’ metallic screening is very strong, in fact, strong enough to completely overwhelm the extended Coulomb repulsion, once a sufficient amount of doping and sufficient electronic background screening, with $x > 5\%$ and $\epsilon_B \gtrsim 4$, say, is present. Additional background screening due to phonons will not have any significant effect on V_S under these conditions.

From the foregoing discussion, it also becomes clear that the presence and frequency dependence of the phonon contribution to ϵ_B will not substantially affect the Hubbard electrons’ metallic screening at finite doping. If one were to include a phononic frequency dependence in ϵ_B , with a typical phonon frequency scale $\Omega_{ph} \ll 8t$, then as a function of $i\omega$, one would find that $V_S(r, i\omega)$ is given roughly by the pure Hubbard result (*i.e.* the dashed lines in Fig. 1) at frequencies $|i\omega| \ll \Omega_{ph}$ where the phonons contribute to the background screening; and $V_S(r, i\omega)$ is given roughly by the extended Hubbard result with $\epsilon_B \cong 4$ (*i.e.* by the full lines in Fig. 1) at frequencies $|i\omega| \gtrsim \Omega_{ph}$ where the phonons do not contribute to the background screening. Over most of the doping range of interest, *e.g.*, between $x \sim 10\%$ and $x \sim 20\%$, this additional “phononic” frequency dependence of V_S , for $|i\omega|$ on the scale of Ω_{ph} , is thus quite small, since the $\epsilon_B = 4.0$ extended Hubbard results are not very different the $\epsilon_B = \infty$ pure Hubbard results for V_S . More importantly, the qualitative features of V_S , such as its doping dependence and the overscreening effects at finite doping will not be changed by the phononic effects. The foregoing argument implicitly assumes that the characteristic frequency scale of the electronic density correlations, *i.e.*, of $\chi_o(q, i\omega)$, is much higher than Ω_{ph} . From earlier QMC studies, it appears that this condition is indeed satisfied, since the spectral weight for density fluctuations in the Hubbard model extends over a frequency range comparable to the electronic bandwidth.²⁰

By the same arguments, the phononic frequency dependence of V_S will become increasingly important at low doping concentrations where the metallic screening of the Hubbard electrons is too weak to suppress the extended Coulomb effects. This observation may offer a possible explanation for the doping dependence of the isotope effect in the superconducting transition temperature of the cuprates. The observed isotope exponent²¹ α is generally a decreasing function of doping, in the underdoped regime, and becomes negligibly small (compared to the classical BCS value of $\alpha = \frac{1}{2}$) in the “optimal” doping range near $x \sim 15\%$. This behavior is qualitatively consistent with the notion that, with increasing

doping, the phonon effect becomes less and less important in the screened potential. Along with its doping dependence, also the overall magnitude of the isotope exponent in underdoped cuprates (which can exceed the classical BCS value²¹) has been a long-standing theoretical puzzle,²² given the assumption of an electronic pairing mechanism. It remains to be explored within specific pairing models whether the phononic frequency dependence of the screened Coulomb potential is large enough to also explain the observed magnitudes of α in the underdoped regime.

Minus sign problems at finite doping unfortunately limit our simulations to $T \geq 0.33t$. However, at least in that temperature regime, we find $|V_S|$ to be increasing with decreasing T . This suggests that the overscreening effects (*i.e.* the attraction in $V_S < 0$) becomes stronger than shown in Fig. 1 at lower T .

The presence of *both* a strong Hubbard- U and finite doping density $x > 0$ are crucial for these overscreening effects to arise. If we replace the fully V_o -renormalized P_o in (4) by, say, the non-interacting ("RPA") polarization bubble P_{RPA} , we also obtain a suppression of $V_S(r)$. However, both the on-site ($r=0$) and the short-range extended part ($r \neq 0$) of V_S remain repulsive in RPA over the whole doping range studied here.²³

In the undoped large- U system, $V_S(r)$ is reduced relative to $V(r)$, by a roughly r -independent factor comparable to the ratio ϵ_{ex}/ϵ_B , for $r \neq 0$, *i. e.* V_S is reduced relative to V but retains a repulsive $1/|r|$ -dependence. This is expected for the screening of a $1/|r|$ potential in an insulator and confirms the insulating character of the $\frac{1}{2}$ -filled Hubbard system. The $1/r$ long-distance behavior of $V_S(r)$ can of course again be traced back to the fact that long-wavelength charge fluctuations are suppressed in the $\frac{1}{2}$ -filled insulating state. For $x = 0$, $\chi(q, i\omega) \sim |q|^2 \rightarrow 0$, and hence also $P(q, i\omega) \sim |q|^2 \rightarrow 0$ for $|q| \rightarrow 0$. As a consequence, the screening denominator $1 - V(q)P(q, i\omega)$ in Eq. (4) remains finite for $q \rightarrow 0$ and $V_S(q, i\omega)$ inherits the $1/|q|^2$ singularity of $V(q)$, thus its $1/|r|$ -dependence upon Fourier transforming back to r -space.

By contrast, in the doped system, the screening takes on a noticeably metallic character and the r -dependence of V_S changes dramatically, even on the finite lattice sizes and high temperatures accessible with our QMC approach. Already at small doping concentrations, $x \gtrsim 5\%$, $V_S(r, i\omega)$ dies out much faster with $|r|$ than in the undoped case. For example, at "optimal doping" where the 1st neighbor V_S is maximally attractive, the in-plane 2nd neighbor V_S [at $r = (a, a, 0)$] is about 4 times smaller in magnitude than the in-plane 1st neighbor V_S [at $r = (a, 0, 0)$].

The metallic screening also strongly suppresses the inter-layer Coulomb repulsion, with V_S at the nearest inter-layer distance $r = (a/2, a/2, d)$ being reduced by a factor of probably more than 500 relative to the bare V at that distance and by a factor of more than 100 relative to the in-plane 1st neighbor V_S . Notice here that

the quasi-2D Hubbard electron system *can* produce inter-layer screening even though our model does *not* include any matrix elements for inter-layer electron transfer. Unlike the in-plane components of V_S , its inter-layer components remain repulsive at finite dopings, over the doping range explored in Fig. 1, *i.e.*, we do not find any evidence for inter-layer overscreening.

The essential features of V_S are robust against substantial modifications of the extended Coulomb terms. Note here that, in real materials, the simple $1/|r|$ -dependence of $V_e(r)$ will of course be modified locally by local field effects.^{10,23} However, our results do not change by more than 20 – 30% if we in- or decrease $V_e(r)$ locally, at 1st, 2nd, and/or 3rd neighbor distances, by up to 30%, relative to Eq. (2). The latter is a conservative upper limit for such local field effects, based on the cuprates' Wannier orbital and crystal structure.^{4,10,23} Using different layered 3D geometries, such as a $YBa_2Cu_3O_7$ bi-layer structure, also does not change the results in Fig. 1 by more than a few percent.

We have also carried out QMC simulations with the 1st neighbor extended Hubbard model, Eq. (10), at finite doping, thereby including extended Coulomb effects in our in our polarization insertion P . Surprisingly, we find that this actually increases the 1st neighbor attraction of V_S and, to a lesser extent, also the on-site attraction. For example, if we simulate and analyze according to Eqs. (4,8) an in-plane 1st neighbor Hubbard model, with $V(r) = V_o(r)$ given by Eq. (10) and a 1st neighbor repulsion strength $V_1 = 0.5t = 0.175\text{eV}$, then the magnitude of the 1st neighbor attraction in $V_S(r, i\omega = 0)$ at a near-optimal doping of $x = 14\%$ increases by about 16% relative to the pure on-site Hubbard model results shown in Fig. 1(c). Notice that this is a comparison of two exact results, since we have used the same potential $V(r)$ in Eq. (4) as was used as our QMC potential $V_o(r)$, both in the pure Hubbard and in the 1st neighbor extended Hubbard calculation, *i.e.* $\chi_o = \chi$ and $P_o = P$ exactly. The foregoing result implies that the 1st neighbor overscreening (in the 5 – 25% doping range) is not only robust against extended Coulomb interactions, but, in fact, could be enhanced if extended Coulomb interactions are included exactly in the polarization insertion. This result also suggests the interesting possibility that extended Coulomb interactions may actually contribute constructively to the pairing attraction for extended superconducting pair wavefunctions,²⁴ and specifically to $d_{x^2-y^2}$ -pairing, as discussed in Section VI. The effects of including extended Coulomb interactions in the polarization insertion need to be investigated further. Specifically, the effects of longer-range Coulomb terms (2nd, 3rd, ...) neighbor need to be explored.

Only at unphysically large V_1 , *i.e.* unphysically small ϵ_B , does our approach break down, due to charge density wave instabilities. These instabilities are signaled by $1/\chi(q, i\omega = 0) \rightarrow 0$ at some point in q -space. For the parameter range explored in the present paper, this occurs only for $\epsilon_B \lesssim 2.0$.

V. EXACT PROOF OF ON-SITE OVERSCREENING AND ITS IMPLICATIONS FOR THE POLARIZATION INSERTION

In order to see why a sufficiently large U at finite doping $x \equiv 1 - \langle n_j \rangle$ *must* cause an on-site overscreening effect, we consider first the pure Hubbard model, $V(r) \equiv U\delta_{r,0}$, where, from the *exact* Eq. (4),

$$V_S(r, i\omega) = U\delta_{r,0} - U^2\chi(r, i\omega), \quad (26)$$

with $V_S(r, i\omega)$ and $\chi(r, i\omega)$ denoting the respective Fourier transforms of $V_S(q, i\omega)$ and $\chi(q, i\omega)$ back into r -space. Clearly, the on-site $-U^2\chi$ -term in Eq. (26) is attractive for all $i\omega$, since $\chi(r=0, i\omega)$, the autocorrelation function of Δn_j , is always positive.

At $x=0$, *i.e.* in the $\frac{1}{2}$ -filled insulator, charge fluctuations are suppressed by the Mott-Hubbard gap. For $U \rightarrow \infty$, one finds from a large- U expansion that $\chi(r, i\omega=0) \sim \mathcal{O}(t^2/U^3)$, and, in Eq. (26), $V_S(r=0, i\omega=0) \cong U - \mathcal{O}(t^2/U) > 0$ which remains repulsive for large $U \gg t$. The crucial point here is that, at finite $|x| > 0$, even an infinitely large U can *not* completely suppress the charge fluctuations, since n_j is not conserved at finite $|x|$, regardless of U . Specifically, the on-site component $\chi(r=0, i\omega)$ approaches a positive, *non-zero* limit [of $\mathcal{O}(x/t)$, by a simple $U = \infty$ scaling argument] for $U \rightarrow \infty$. Hence, the $-U^2\chi$ -term will overcome the bare U -term in (26) and $V_S(r=0, i\omega)$ must become attractive, *i.e.* on-site overscreening must occur, for sufficiently large U . Also, as a consequence, for sufficiently large U , $V_S(r=0, i\omega=0)$ *must* change sign as a function of x .

Formally, the suppression of χ at $\frac{1}{2}$ -filling arises in the strong-coupling expansion because the large repulsive U effectively projects out the low-energy Hilbertspace sector containing only states without doubly occupied sites. Upon projection onto the low-energy sector, the on-site charge operators n_j become exactly conserved with $n_j = 1$ and $\Delta n_j = 0$ at all sites for $U \rightarrow \infty$, giving $\chi \equiv 0$ from Eq. (6). At large, but finite U , intersite charge transfer processes via the hybridization term H_t , must necessarily go through “virtual” intermediate states containing at least one doubly occupied site. To 2nd order in the hybridization H_t , each of the two matrix elements exciting from the low-energy sector into this high-energy sector and back is of order t/U while the inverse energy denominator associated with the virtual excitation is of order $1/U$, resulting in $\chi \sim t^2/U^3$. At finite doping, on the other hand, the projected n_j are not conserved. Even for $U = \infty$, the doping induced holes can still move through the lattice, via the H_t -term, since the intersite charge transfer can proceed without having to go through high-energy intermediate states involving double occupancy. Hence, χ approaches a non-zero limit, $\chi_\infty \neq 0$, at finite doping concentration for $U \rightarrow \infty$.

Note that the foregoing large- U argument constitutes an *exact* analytical proof of on-site overscreening in the

asymptotic limit $U \rightarrow \infty$. The proof holds both on finite and infinite lattices in any spatial dimension and it immediately generalizes to the full extended Hubbard model, Eqs. (1,2) since the $-U^2\chi$ -term remains the dominant screening contribution for $U/t \rightarrow \infty$ at finite $x > 0$, even in the presence of a finite extended interaction term $V_e \neq 0$. Our QMC results in Fig. 1a not only confirm these exact large- U results; they also show that the large- U scenario is realized in the physically relevant parameter regime⁴ $U \sim 8 - 12t$.

The occurrence of on-site overscreening, or close proximity to it, is accompanied by profound effects in the polarization insertion $P(q, i\omega)$, namely, by q -dependent singularities of P on the (analytically continued) $i\omega$ -axis. To see this, recall that $V_S(r=0, i\omega)$ is just the Brillouin zone average of $V_S(q, i\omega)$. Hence, in order to get $V_S(r=0, i\omega) < 0$, there must be some region in q -space, for which $V_S(q, i\omega) < 0$. On the other hand, since $\chi(q, i\omega) \sim \mathcal{O}(1/\omega^2)$ for $|i\omega| \rightarrow \infty$, it follows from Eq. (4) that $V_S(q, i\omega) \rightarrow V(q) > 0$ for $|i\omega| \rightarrow \infty$, *i.e.*, in the high frequency limit the screened potential approaches the repulsive bare potential. Hence, for those q for which $V_S(q, i\omega) < 0$ at some (low) frequency $i\omega$, there must exist at least one $i\omega^{(s)}(q)$, on the imaginary frequency axis, such that $V_S(q, i\omega)$, analytically continued onto the continuous $i\omega$ -axis, goes through zero,

$$\lim_{i\omega \rightarrow i\omega^{(s)}(q)} V_S(q, i\omega) = 0. \quad (27)$$

By Eq. (4), this implies

$$\lim_{i\omega \rightarrow i\omega^{(s)}(q)} 1/\chi(q, i\omega) = V(q) \quad (28)$$

and, by Eq. (5) which is equivalent to $1/P(q, i\omega) = V(q) - 1/\chi(q, i\omega)$, this implies

$$\lim_{i\omega \rightarrow i\omega^{(s)}(q)} 1/P(q, i\omega) = 0. \quad (29)$$

In other words, $1/P(q, i\omega)$ changes sign and $P(q, i\omega)$ must be singular at $i\omega^{(s)}(q)$.

Note that this is clearly a strong correlation effect. Weak coupling approximations to $P(q, i\omega)$, notably RPA, do not give such a singularity in $P(q, i\omega)$. In RPA, $1/P(q, i\omega) < 0$ at all q and $i\omega$. It is therefore not surprising that RPA cannot reproduce the on-site overscreening effect. Note also that this singularity in P does not imply any singularities (*i.e.* instabilities) in physically observable quantities, such as $\chi(q, i\omega)$. In fact, $\chi(q, i\omega)$ is perfectly regular at $i\omega^{(s)}(q)$, as implied by Eq. (28) and $V(q) > 0$.

However, the singularity of $P(q, i\omega)$ does imply singularities of certain vertex functions to which both P and the single-particle self-energy Σ are diagrammatically related. For example, both P and Σ can be expressed in terms of an appropriately defined 3-point vertex function $\Lambda(k, i\nu; q, i\omega)$, with entering boson momentum-energy $(q, i\omega)$, entering fermion momentum-energy $(k, i\nu)$ (where $i\nu$ is an odd Matsubara frequency)

and exiting fermion momentum-energy ($k + q, i\nu + i\omega$), such that⁵

$$P(q, i\omega) = \left(\frac{T}{N}\right) \sum_{k, i\nu} G(k, i\nu) G(k + q, i\nu + i\omega) \Lambda(k, i\nu; q, i\omega) \quad (30)$$

and

$$\begin{aligned} \Sigma(k, i\nu) &= \Sigma_H(k) \\ &- \left(\frac{T}{N}\right) \sum_{q, i\omega} V_S(q, i\omega) G(k + q, i\nu + i\omega) \Lambda(k, i\nu; q, i\omega) \quad (31) \end{aligned}$$

where $G(k, i\nu)$ is the single-particle Green's function and Σ_H denotes the self-energy contribution from the Hartree diagram. Note that the singularity of P implies an analogous singularity in the $i\omega$ -dependence of Λ for $i\omega \rightarrow i\omega^{(s)}(q)$. However, in the foregoing expression for Σ , which is, in principle, a physically observable quantity, the singularity of Λ is cancelled by the vanishing of the other factor in the summand, $V_S(q, i\omega) \rightarrow 0$ for $i\omega \rightarrow i\omega^{(s)}(q)$. The formal implications of this singularity in P and Λ need to be further investigated.

As discussed in Section IV, RPA results show that, for near (1st, 2nd, ...) neighbor r 's, $\chi(r, i\omega = 0)$ is negative at small U , whereas QMC results suggest that the near-neighbor $\chi(r, i\omega = 0)$ becomes positive at finite doping when U exceeds a doping dependent threshold of order several t . From Eq. (26) one sees that this positive near neighbor $\chi(r, i\omega = 0)$ gives rise to the near neighbor attraction in V_S at large U and finite x , as displayed in Fig. 1b. Hence, the QMC and RPA results taken together suggest that near-neighbor overscreening is fundamentally also a large- U effect, just like on-site overscreening. However, note here that $\chi(r, i\omega)$ for $r \neq 0$ is *not* an autocorrelation function and its sign is allowed to be either positive or negative, depending on the model parameters. Because of this, it does not seem to be possible to generalize the above large- U overscreening proof to show the existence of near- (1st 2nd, ...) neighbor overscreening in $V_S(r, i\omega)$ by analytical means. Also, unlike the on-site overscreening case, the existence of near-neighbor overscreening does not necessarily imply the existence of singularities in $P(q, i\omega)$.

VI. D- AND S-WAVE PAIRING STRENGTHS

Given the attractive nature of the screened potential at finite doping, it is tempting to ask whether this attraction could give rise to superconductivity and, if so, of what pairing symmetry. A potential advantage of our diagrammatic expansion in the charge representation is the large reduction of the overall strength of V_S in the 10 – 20% doping range, compared to the bare Hubbard- U . This

suggests the possibility of carrying out controlled, self-consistent weak-coupling expansions in which the fully screened V_S , rather than the bare V or U , serves as the small parameter. Such an expansion can be formulated diagrammatically⁵ by retaining only skeleton diagrams in which none of the interaction lines contain any polarization insertions and each interaction line represents a $V_S(q, i\omega)$. Superconducting instabilities can then be studied in terms of such a perturbative approximation to the irreducible particle-particle vertex, expanded to 1st order in V_S .

As a first step in that direction, we have explored possible V_S -induced or -enhanced superconducting pairing instabilities, using the standard Eliashberg-McMillan (EM) approach.²⁵ A convenient measure of the pairing strength of V_S are the dimensionless EM λ -parameters, defined in terms of the Fermi surface "expectation values" of $V_S(k - k', i\omega = 0)$ for relevant Cooper pair trial wavefunctions $\eta(k)$ in electron momentum (k -) space, as described, *e.g.*, in Refs. 13 and 25.

In Fig. 1(c), we show the EM parameters λ_s , for on-site s -wave (and, identically, for in-plane 1st neighbor s -wave),²⁶ and λ_d , for in-plane 1st neighbor $d_{x^2-y^2}$ pairing, with respective pair wavefunctions $\eta_s(k) \equiv 1$ and $\eta_d(k) = \cos(ak_x) - \cos(ak_y)$. To carry out the required Fermi surface integrals, our 3D $V_S(q, i\omega)$ was interpolated from the finite $8 \times 8 \times 8$ lattice q -grid onto a $200 \times 200 \times 200$ q -grid, using the 3D version of the q -interpolation scheme described in Section III for the 2D q -interpolation of χ_o . Applying this interpolation scheme to $V_S(q, i\omega)$ is justified here, analogous to the above χ_o -interpolation, by the fact that, at finite doping, $V_S(r, i\omega)$ is of very short-range in r -space, due to the "metallic" character of the screening.

At low doping, the dominant attractive ($\lambda > 0$) channel is $d_{x^2-y^2}$ with λ_d reaching a maximum of $\sim 0.15 - 0.17$ near $x \sim 10 - 14\%$. λ_s is repulsive at low doping, but becomes strongly attractive at larger doping $x \gtrsim 15\%$. Thus, as expected on symmetry grounds, λ_s and λ_d reflect the doping dependence of the on-site and 1st neighbor attraction V_S shown in Fig. 1(a) and (b), respectively. We note in passing that the doping dependence of λ_d is reminiscent of the observed doping dependence of the superconducting T_c in the cuprates.² The λ -values for near-neighbor pair wavefunctions of other symmetries (p , d_{xy} , g) are small compared to λ_s and λ_d and for that reason not further discussed here.

The spectral weight of $\chi(q, i\omega)$ extends up to values $\Omega_\chi \sim 8 - 10t$.²⁰ In the EM analysis,²⁵ this "boson" energy scale, together with λ , determines the superconducting T_c , roughly as $T_c \sim \Omega_\chi \exp(-1/\lambda)$. Because of the large Ω_χ -scale, it may be possible, at least within the EM approximation, to achieve high T_c 's even for moderate coupling values $\lambda < 1$.

We should caution here that the foregoing QMC results can of course only suggest the general, qualitative trends in V_S and λ parameters, due to the high temperatures and small lattice size limitations inherent in the QMC

approach. Also, our EM approach is based formally on a perturbative expansion of the exact irreducible particle-particle vertex to 1st order in V_S . This approximation should be relied upon, if at all, only close to the "cross-over" $x_C \cong 15\%$ where $V_S(r=0, i\omega=0) = 0$, so that $|V_S(q, i\omega)| \ll 8t$, at least for low frequencies $|i\omega| \ll 8t$. i.e. roughly in the 10 – 20% doping range. At large over- or underdoping ($x \gtrsim 20\%$ or $x \lesssim 10\%$), where $|\lambda_s| \sim \mathcal{O}(1)$, corrections of higher order in V_S are likely to contribute strongly to the self-energy and to the irreducible particle-particle vertex, thereby causing the EM approximation, with V_S as the effective pairing potential, to break down. The increasingly attractive λ_s -values at $x \gtrsim 25\%$ doping, in Fig. 1c, do therefore not necessarily imply increasingly strong s -wave pairing tendencies. The effects of vertex corrections, of higher order in V_S , need to be further explored, both in the over- and underdoped regimes.

It is also important to realize that the strong reduction in overall screened potential strength $|V_S|$ is only a necessary, not a sufficient condition for the applicability of the EM approach. Note in particular, that V_S is "weak" (and, where applicable, attractive) only at low frequencies. At large frequencies, with $|i\omega|$ of the order of the bandwidth $8t$, the charge correlation function begins to die out, with $\chi(q, i\omega) \sim 1/|i\omega|^2$, and, by Eq. (4), $V_S(q, i\omega) \rightarrow V(q)$ for $|i\omega| \rightarrow \infty$. In other words, at high frequencies, the screened potential recovers the full strength of the bare potential. Physically, this simply reflects the fact that at high frequencies, $|i\omega| \gg 8t$, the conduction electron system is "too slow" to provide a screening response to very rapidly varying fields. Since the characteristic frequency scale of these charge fluctuations is quite high, of the order of the bandwidth,²⁰ the conventional underpinnings of the EM approximation, such as the Migdal theorem, are not necessarily satisfied. Thus, even in the "near-optimal" doping regime where the low-frequency V_S is weak, it needs to be re-examined whether corrections to the irreducible particle-particle vertex of higher order in V_S are indeed small.

With these caveats in mind, we should compare our results for the pairing strengths in the Hubbard model to earlier studies of the superconducting pairing correlations^{27–30} and of the effective pairing potential^{16,17,31,32} in the Hubbard model. Early studies of pair correlation functions^{27–29} and pair bound state symmetries on small lattices^{33,34} using formally exact QMC simulation methods^{27–29,33} and exact diagonalization,³⁴ indicated a tendency towards $d_{x^2-y^2}$ -pairing. In finite- T simulations,^{27–29} this was suggested by an increase in $d_{x^2-y^2}$ pairing correlations with decreasing temperature. However, due to the QMC minus-sign problem, these exact QMC studies were limited to small lattice sizes and rather high temperatures (in physical units about an order of magnitude higher than the observed T_c scale in the cuprates). It may therefore be difficult to draw meaningful conclusions about the low-temperature long-range pairing correlations of the model

from the finite-system and/or finite- T exact QMC data for pair correlation functions.

Also, by contrast, more recent studies of pairing correlations in the groundstate of the Hubbard model, based on the "constrained path Monte Carlo" (CPMC) approach, did not provide any evidence for long-range pairing correlations of either $d_{x^2-y^2}$ - or s -wave symmetry.³⁰ However, the CPMC approach is based on a (in principle uncontrolled) variational approximation which, albeit remarkably successful in reproducing exactly known groundstate energies, may not necessarily reproduce the exact pairing correlations. Thus, existing QMC studies of pair correlation functions in the Hubbard model are, at best, inconclusive as far as $d_{x^2-y^2}$ -pairing is concerned and, with all the above-cited limitations, they do not provide evidence for s -wave pairing in the near- $\frac{1}{2}$ -filled Hubbard model.

In addition to the above-cited "technical" limitations, there is a further, physical reason why especially long-range s -wave pairing correlations, if existent in the Hubbard model, may escape detection in QMC simulations of pair correlation functions. To understand this, note that retardation plays a central role in the physical origin of the overscreening attraction in our V_S . For example, for the pure Hubbard model, Eq. (26), Fourier transformed to the (imaginary) time (τ) domain, becomes

$$V_S(r=0, \tau) = U\delta(\tau) - U^2\chi(r=0, \tau) . \quad (32)$$

A pair of electrons, e and \bar{e} , say, is subject to the instantaneous, bare repulsive U interaction term only if they both occupy the same site j at the same time. By contrast, the attractive screening term, $-U^2\chi$, is retarded, i.e., physically speaking, the charge polarization caused by \bar{e} at site j can still be felt by e after a time lag $\theta > 0$, when \bar{e} has already left j . Thus, the on-site overscreening arises from processes wherein the two electrons interact on the same site, but at different times, via their local charge polarizations, thereby evading their bare, instantaneous repulsion. The time scale for this retarded interaction is governed by the frequency spectrum of the dynamical density correlation χ , i. e., for the relevant parameter range it is of order of the inverse bandwidth $(8t)^{-1}$.²⁰ Pair correlations induced by such a potential, with retarded attractive and instantaneous repulsive contributions, should be most easily detected via *time-delayed* pair creation order parameters of the general form

$$\Delta_\theta = c_{j,\sigma}^\dagger(\theta)c_{j,\bar{\sigma}}^\dagger \quad (33)$$

where $c_{j,\sigma}^\dagger(\theta) \equiv e^{\theta H} c_{j,\sigma}^\dagger e^{-\theta H}$. In other words, Δ_θ creates the second electron e with time lag θ relative to the first electron \bar{e} . For the on-site s -wave ($j = \bar{j}$) case, one should thus consider time-delayed pair correlation functions of the general form

$$C(r_j - r_{j'}, \tau, \theta, \theta') = \langle T [c_{j\downarrow}(\tau + \theta) c_{j\uparrow}(\tau) c_{j'\uparrow}^\dagger(\theta') c_{j'\downarrow}^\dagger(0)] \rangle \quad (34)$$

where $T[\dots]$ implies fermion time ordering. The strongest signal for pairing correlations should then be detected for typical values of θ and θ' which are comparable to the retardation time scale of the attractive part of the potential, *i.e.*, in the case of our $V_S(r, \tau)$, for $\theta, \theta' \sim (8t)^{-1}$. By contrast, the existing QMC studies of pairing correlation functions in the Hubbard model have so far considered only *simultaneous* pair correlations $C(r_j - r_{j'}, \tau, \theta, \theta')$ with $\theta = \theta' = 0$. In such a simultaneous pair correlation function, the detectable signal for *s*-wave pairing is expected to be very weak (and, in the case of pairing with odd frequency parity, identically zero) if the underlying pairing potential happens to have a time-dependent structure of the sort described above for $V_S(r, \tau)$, *i.e.* a strong instantaneous repulsion superimposed on a retarded attraction. We note that for such a temporal structure of the pairing potential the possibility of a triplet *s*-wave pairing state with odd frequency parity³⁵ can not be ruled out.

In using QMC simulations to find superconducting instabilities via the pair correlation function approach one thus faces at least three major difficulties: (i) long-range pair correlations develop only at low temperatures, of order T_c ; (ii) it requires large lattice sizes to detect such long-range correlations in finite systems (a problem compounded at finite T in two dimensions by the expected algebraic decay of the correlations); and, (iii) depending on the structure of the superconducting order parameter, the simulated pair correlation function may provide only an undetectably weak signal if one chooses the “wrong” pair creation operators (and one doesn’t know *a priori* which operators are the “right” ones). A potentially promising route to circumvent some of these difficulties is to focus instead on the underlying exact effective pairing *potential*, *i.e.* in precise diagrammatic terms, on the irreducible particle-particle vertex function.^{16,17,31,32} The basic idea here is that, in contrast to long-range pair correlations, the effective pairing potential may be (i) of short range and may (ii) develop strong signatures of the pairing attraction already at high temperatures. Also, (iii) by solving for the dominant pairing eigenvalues and eigenfunctions of the the corresponding particle-particle ladder equation, the particle-particle vertex approach automatically reveals the symmetry and space-time structure of the dominant superconducting order parameter.

The existing QMC results for the exact irreducible particle-particle vertex of the 2D Hubbard model near $\frac{1}{2}$ -filling suggest that there is indeed a noticeable 1st neighbor pairing attraction and that a pairing eigenfunction of spin-singlet $d_{x^2-y^2}$ symmetry becomes dominant (*i.e.*, develops the largest pairing eigenvalue) as the temperature is lowered.^{16,32} In addition, sub-dominant pairing eigenvalues of comparable magnitude with eigenfunctions of odd-frequency triplet *s*- and odd-frequency singlet *p*-wave symmetry are found.¹⁶ The effective “on-site” interaction extracted from the irreducible particle-particle vertex is found to be repulsive.¹⁷

We should emphasize here that, aside from some pre-

liminary studies at $\frac{1}{2}$ -filling,³² all of the foregoing exact irreducible particle-particle vertex results were obtained at a doping concentration of $x \cong 13\%$ and, at that concentration, they are *not* inconsistent with our results for the pairing λ -parameters shown in Fig. 1(c). At $x = 13\%$, our $d_{x^2-y^2-\lambda}$ is indeed the dominantly attractive one; the *s*-wave- λ is repulsive at $x = 13\%$ and becomes attractive only for $x > 15\%$.

Also, unfortunately, the reported results for the real-space interaction strengths extracted from the irreducible particle-particle vertex¹⁷ were reported for smaller Hubbard U , $U = 4t$, whereas a physically more realistic larger value of $U = 8t$ was used in our calculations of $V_S(r, i\omega)$. Recall here that, as discussed above, the on-site overscreening is a large- U effect and $U = 4t$ may simply be too small to produce on-site overscreening. Interestingly, from a comparison of the pairing eigenvalues extracted from the irreducible particle-particle vertex at $U = 4t$ and at $U = 8t$,¹⁶ it appears that the (odd frequency triplet) *s*-wave eigenvalues are *increasing* with U . This observation is not inconsistent with the notion that one moves towards on-site overscreening with increasing U .

It would therefore be of considerable interest to check whether the irreducible particle-particle vertex develops an on-site attraction and stronger *s*-wave pairing tendencies at larger doping, $x > 15\%$, and larger Hubbard repulsion U , *e.g.*, for $U = 8t$. This would provide a very stringent test as to whether our screened potential V_S in the charge representation indeed provides a reasonable approximation to the exact irreducible particle-particle vertex or whether particle-particle vertex corrections of higher order in V_S are important.

In analyzing the irreducible particle-particle vertex, it was also found that its momentum and real-space structure, and the T -dependence of that momentum and real-space structure, closely resembles that of an appropriately defined spin fluctuation mediated pairing potential of the Hubbard model, suggesting that spin fluctuations are indeed responsible for the *d*-wave pairing attraction.^{17,31} It is possible that the positive near-neighbor charge correlations [*i.e.* $\chi(r, i\omega = 0) > 0$ at near-neighbor r -vectors], responsible for the *d*-wave pairing attraction in our approach, are closely (and perhaps causally) related to short-range antiferromagnetic spin correlations in Hubbard systems near $\frac{1}{2}$ -filling. The charge representation approach developed here may thus provide a description of the physics in near- $\frac{1}{2}$ -filled Hubbard systems which is complementary to that of a spin fluctuation-based approach.^{2,36,37} The overscreening of the on-site potential, and hence the possibility of *s*-wave pairing in the Hubbard model, is one aspect of this problem which may be (with all the above-stated caveats!) “obvious” in the former, but difficult to reproduce in the latter approach. The relationship between our charge representation formulation and the spin fluctuation picture of the Hubbard model^{2,36,37} needs to be further investigated.

VII. SUMMARY

In summary, by a combination of diagrammatic and quantum Monte Carlo techniques and by exact analytical approaches, we have studied the dielectric screening and the screening of electron-electron Coulomb repulsions in the charge representation of the 2D Hubbard and of the quasi-2D extended Hubbard models relevant to the cuprate superconductors.

Applying a combination of QMC simulations and diagrammatic techniques, we have calculated the contribution of the quasi-2D extended Hubbard electron system at $\frac{1}{2}$ -filling to the long-wavelength in-plane dielectric screening in the undoped insulating cuprate parent compounds. Combining this result with experimental data for the observed long-wavelength dielectric tensor in the La_2CuO_4 , we have then obtained an estimate for the strength of the dielectric screening due the insulating “background” of non-Hubbard electrons and phonons and, thereby, for the effective strength of the extended $1/|r|$ Coulomb interaction potential in the Hubbard conduction electron system. Our results imply that no more than 25% of the observed electronic in-plane dielectric constant (ϵ_∞) arises from the $\frac{1}{2}$ -filled Hubbard conduction electron system.

Using again a combination of diagrammatic and QMC techniques, we have then studied the effective, screened electron-electron interaction potential V_S , as a function of doping x , in the both the 2D Hubbard and quasi 2D extended Hubbard model. We find that finite doping gives rise to overscreening effects which cause V_S to become attractive at finite doping concentrations. Specifically, we find that the low-frequency extended (1st, 2nd... neighbor) part of V_S , while repulsive and rapidly suppressed with doping at small x , becomes attractive for $x \gtrsim 5\%$. Near $x \sim 10 - 15\%$, the extended part of V_S exhibits maximum attraction strength and, for $x \gtrsim 20 - 25\%$, it becomes repulsive again and increases with x . At larger doping, $x \gtrsim 15\%$, even the on-site part of V_S changes sign and becomes attractive, with a monotonic x -dependence between $x = 0$ and $x = 30\%$.

Both spatially extended (1st, 2nd, ... neighbor) and on-site overscreening effects are robust against the presence of and moderate changes in the 3D extended $1/|r|$ Coulomb repulsions, and largely independent of the arrangement of CuO_2 -layers in the 3D crystal structure. Generally, at doping concentrations larger than 5 – 10%, our results for the screened interaction potential of the extended Hubbard model, with extended $1/|r|$ Coulomb interactions of realistic strength, differ from those of the pure 2D Hubbard model (with only on-site U repulsion) by no more than 10 – 20%. This suggests that the extended Coulomb effects do not qualitatively alter the short-range charge correlations and screening in the Hubbard electron system at finite doping near $\frac{1}{2}$ -filling. In particular the overscreening effects which we find at doping concentrations $x \gtrsim 5\%$ are intrinsic to the pure 2D

Hubbard model. These overscreening effects are modified, but neither caused nor destroyed by the extended Coulomb terms. When included exactly in the screening calculation, a repulsive 1st neighbor extended Coulomb term enhances the 1st neighbor overscreening in V_S at finite doping, suggesting the possibility that repulsive extended Coulomb terms could actually contribute to an extended pairing attraction.

Independent of the QMC results, we have presented an exact analytical proof that, in the large- U limit, doping induced charge fluctuations must give rise to an “overscreening” effect which causes the *exact* screened on-site Coulomb potential V_S in the charge representation to become attractive. We have shown that this is indeed an intrinsic local property of both large- U Hubbard and extended Hubbard models at finite doping which exists independent of dimensionality, 3D crystal structure or system size. Our QMC results thus show that this asymptotic large- U scenario is indeed realized in the finite- U parameter range relevant to the cuprates. We have also shown that on-site overscreening implies singularities in the imaginary-frequency dependence of the irreducible polarization insertion and of its underlying 3-point vertex function.

When analyzed as an effective pairing potential *i.e.* formally, as a 1st order approximation to the irreducible particle-particle vertex, the screened potential V_S gives rise to a 1st neighbor $d_{x^2-y^2}$ pairing attraction in the doping range between $x \gtrsim 5\%$ and $x \lesssim 20 - 25\%$ and to an on-site s -wave pairing attraction for $x > 15\%$. The doping dependence of the $d_{x^2-y^2}$ Eliashberg λ -parameter closely tracks that of the extended (1st neighbor) attraction of V_S , with a maximum of pairing strength near $x = 10 - 15\%$, reminiscent of the observed doping dependence of the superconducting T_c in the cuprates. The doping dependence of the on-site s -wave λ -parameter closely tracks that of the on-site V_S , increasing monotonically with x and becoming strongly attractive for $x \sim 15\%$. This suggests the possibility of a doping induced transition or cross-over from d - to s -wave pairing. We have argued that retardation plays an essential role in the on-site overscreening of the interaction potential and that this should be reflected in the temporal / frequency structure of the corresponding s -wave superconducting order parameter.

ACKNOWLEDGMENTS

We would like to acknowledge discussions with D. Emin, G. Esirgen, K. Levin, D. Scalapino, S.K. Sinha, and M.G. Zacher. This work was supported at the University of Georgia by NSF Grants No. DMR-9215123 and DMR-9970291, in part, at the University of California at Santa Barbara by NSF Grant No. PHY99-07949, and at Universität Würzburg by BMBF (05SB8WWA1) and by DFN Contract No. TK 598-VA/D03. Computing

resources from UCNS at the University of Georgia, from HLRZ Jülich and from HLRS Stuttgart are gratefully acknowledged.

-
- ¹ D. J. van Harlingen, *Rev. Mod. Phys.* **67**, 515 (1995).
² D. J. Scalapino, *Phys. Rep.* **250**, 329 (1995).
³ C. C. Tsuei and J. R. Kirtley, *Phys. Rev. Lett.* **85**, 182 (2000); J. D. Kokales *et al.*, cond-mat/0002300; J. D. Kokales *et al.*, cond-mat/0001166; R. Prozorov *et al.*, cond-mat/9912001.
⁴ H.-B. Schüttler and A.J. Fedro, *Phys. Rev. B* **45**, 7588 (1992); and references therein.
⁵ G. D. Mahan, *Many-Particle Physics*, 2nd ed. (Plenum Press, New York, 1990); J. W. Negele and H. Orland, *Quantum Many-Particle Systems*, (Addison Wesley, Redwood City, CA, 1988); A. L. Fetter and J. D. Walecka, *Quantum Theory of Many-Particle Systems* (McGraw-Hill, New York, 1971); A. A. Abrikosov, L. P. Gorkov, and I. E. Dzyaloshinski, *Methods of Quantum Field Theory in Statistical Physics*, (Prentice-Hall, Englewood Cliffs, NJ, 1963).
⁶ J. D. Jorgensen *et al.*, *Phys. Rev. Lett.* **58**, 1024 (1987).
⁷ C. Y. Chen *et al.*, *Phys. Rev. B* **43**, 392 (1991);
⁸ J. P. Falck *et al.*, *Phys. Rev. B* **48**, 4043 (1993).
⁹ H.-B. Schüttler (unpublished).
¹⁰ S. L. Adler, *Phys. Rev.* **126**, 413 (1962); N. Wiser, *ibid.* **129**, 62 (1963); S. K. Sinha, *ibid.* **177**, 1256 (1969); L. J. Sham *Phys. Rev. B* **6**, 3584 (1972); W. Hanke, *ibid.* **8**, 4585 (1973); W. Hanke and L. J. Sham, *Phys. Rev. Lett.* **33**, 582 (1974); S. K. Sinha, *CRC Critical Reviews in Solid State Sciences* **3**, 273 (1973); and references therein.
¹¹ D. Emin, *Phys. Rev. Lett.* **62**, 1544 (1989).
¹² A. Millis, H. Monien, and D. Pines, *Phys. Rev. B* **42**, 167 (1990); P. Monthoux, A. V. Balatsky, and D. Pines, *Phys. Rev. Lett.* **67**, 3448 (1991); *Phys. Rev. B* **46**, 14803 (1992); P. Monthoux and D. Pines, *Phys. Rev. Lett.* **69**, 961 (1992); *Phys. Rev. B* **47**, 6069 (1993); *ibid.* **49**, 4261 (1994).
¹³ H.-B. Schüttler and M. N. Norman, *Phys. Rev. B* **54**, 13295 (1996).
¹⁴ Including a 1st neighbor repulsion V_1 of the strength estimated here into the phenomenological spin fluctuation exchange models of Ref. 12 would suppress the transition temperatures for d -wave in these models by typically a factor of 2 or more [J. Cao and H.-B. Schüttler (unpublished)].
¹⁵ E. Dagotto, *Rev. Mod. Phys.* **66**, 763 (1994).
¹⁶ N. Bulut, D. J. Scalapino, and S. R. White, *Phys. Rev. B* **47**, 6157 (1993).
¹⁷ N. Bulut, D. J. Scalapino, and S. R. White, *Phys. Rev. B* **50**, 9623 (1994).
¹⁸ Pairing mechanisms based on the t - J model will certainly not survive without, and just barely with, the phonon part of ϵ_B , a point perhaps overlooked in some recent work proposing a “purely electronic mechanism” in the t - J model context; see *e.g.* C. Gazza *et al.*, cond-mat/9803314.
¹⁹ A notable exception here is the fluctuation exchange approximation treatment of the Hubbard model where the d -wave T_c due to spin fluctuations is found to be *not* significantly suppressed by the inclusion of substantial V_1 - and longer-range Coulomb repulsion terms of the magnitude estimated here, *c.f.* Ref. 37.
²⁰ R. Preuss *et al.*, *Phys. Rev. Lett.* **79**, 1122 (1997).
²¹ M.K. Crawford *et al.*, *Phys. Rev. B* **41**, 282 (1990); *Science* **250**, 1390 (1990); J.P. Franck *et al.*, *Physica C* **185-189**, 1379 (1991); *Phys. Rev. Lett.* **71**, 283 (1993); J. P. Franck in *Physical Properties of High T_c Superconductors IV*, D. M. Ginsberg (editor), p. 189 (World Scientific, 1994); J. P. Franck and D. D. Lawrie, *Physica C* **235-240**, 1503 (1994); *J. Supercond.* **8**, 591 (1995); J. P. Franck, *Physica Scripta* **T66**, 220 (1996).
²² H.-B. Schüttler and C.-H. Pao, *Phys. Rev. Lett.* **75**, 4504 (1995); C.-H. Pao and H.-B. Schüttler, *J. Supercond.* **8**, 633 (1995); *J. Phys. Chem. Solids* **56**, 1745 (1995); *Phys. Rev. B* **57**, 5051 (1998); *ibid.* **60**, 1283 (1999).
²³ D. Z. Liu and K. Levin [*Physica C* **275**, 81 (1997)] find a weak $d_{x^2-y^2}$ pairing attraction from RPA-screened Coulomb matrix elements, due to local field effects.
²⁴ A. J. Leggett, *J. Phys. Chem. Solids* **59**, 1729 (1998); A. J. Leggett, *Phys. Rev. Lett.* **83**, 392 (1999); A. J. Leggett, *Proc. Natl. Acad. Sci. (USA)* **96**, 8365, (1999).
²⁵ P. B. Allen and B. Mitrovic, in *Solid State Physics*, eds. H. Ehrenreich *et al.*, Vol 37, pp. 1-91, Academic Press (New York, 1982).
²⁶ The non-interacting Fermi surface of the in-plane 1st neighbor tight-binding band is a locus of k -points where $\cos(ak_x) + \cos(ak_y) = \text{const}$. The in-plane 1st neighbor extended s -wave pair wavefunction $\eta_{s1}(k) = \cos(ak_x) + \cos(ak_y)$ is therefore constant on that Fermi surface and gives exactly the same value for the EM λ -parameter as the on-site s -wave pair wavefunction $\eta_s(k) = 1$.
²⁷ S. R. White *et al.*, *Phys. Rev. B* **39**, 839 (1989).
²⁸ M. Imada and Y. Hatsugai, *J. Phys. Soc. Jpn.* **58**, 3752 (1989); N. Furukawa and M. Imada, *ibid.* **60**, 3604 (1991).
²⁹ A. Moreo and D. J. Scalapino *Phys. Rev. B* **43**, 8211 (1991); A. Moreo *ibid.* **45**, 5059 (1992).
³⁰ S. Zhang, J. Carlson, and J. E. Gubernatis, *Phys. Rev. Lett.* **78**, 4486 (1997); M. Guerrero, G. Ortiz, and J. E. Gubernatis, *Phys. Rev. B* **59**, 1706 (1999).
³¹ D. J. Scalapino, *Turk. J. Phys.* **20**, 560 (1996); T. Dahm and D. J. Scalapino, *Physica C* **288**, 33 (1997).
³² N. Bulut, D. J. Scalapino, and S. R. White, *Phys. Rev. B* **47**, 14599 (1993).
³³ E. Dagotto *et al.*, *Phys. Rev. B* **41**, 811 (1990).
³⁴ A. Parola *et al.*, *Phys. Rev. B* **43**, 6190 (1991).
³⁵ V. L. Berezinskii, *Pis'ma Zh. Eksp. Teor. Fiz.* **20**, 628 (1974) [*JETP Lett.* **20**, 287 (1974)].
³⁶ N. E. Bickers, D.J. Scalapino, and S. R. White, *Phys. Rev. Lett.* **62**, 961 (1989); N. E. Bickers and S. R. White, *Phys. Rev. B* **43**, 8044 (1991); N. E. Bickers and D. J. Scalapino, *Ann. Phys.* **193**, 206 (1989).
³⁷ G. Esirgen, H.-B. Schüttler, and N. E. Bickers, *Phys. Rev. Lett.* **82**, 1217 (1999).